

Supplementary Information:

Pushing property limits in materials discovery via boundless objective-free exploration

Kei Terayama^{*abcd}, Masato Sumita^{ae}, Ryo Tamura^{efg}, Daniel T. Payne^h, Mandeep K. Chahal^e, Shinsuke Ishihara^e, and Koji Tsuda^{afg}

^aRIKEN Center for Advanced Intelligence Project, 1-4-1 Nihonbashi, Chuo-ku, Tokyo 103-0027, Japan. Email: kei.terayama@riken.jp

^bMedical Sciences Innovation Hub Program, RIKEN Cluster for Science, Technology and Innovation Hub, Tsurumi-ku, Kanagawa 230-0045, Japan.

^cGraduate School of Medicine, Kyoto University, Shogoin-kawaharacho, Sakyo-ku, Kyoto 606-8507, Japan.

^dGraduate School of Medical Life Science, Yokohama City University, 1-7-29, Suehiro-cho, Tsurumi-ku, Yokohama 230-0045, Japan.

^eInternational Center for Materials Nanoarchitectonics (WPI-MANA), National Institute for Materials Science, 1-1 Namiki, Tsukuba, Ibaraki 305-0044, Japan.

^fResearch and Services Division of Materials Data and Integrated System, National Institute for Materials Science, 1-2-1 Sengen, Tsukuba, Ibaraki 305-0047, Japan.

^gGraduate School of Frontier Sciences, the University of Tokyo, 5-1-5 Kashiwa-no-ha, Kashiwa, Chiba 277-8561, Japan. Email: tsuda@u-tokyo.ac.jp

^hInternational Center for Young Scientists (ICYS), National Institute for Materials Science, 1-1 Namiki, Tsukuba, Ibaraki 305-0044, Japan.

Contents

1. Stein novelty

2. Results of BLOX using Lasso, Ridge, SVR, and NN-based models

S1. Sampling result of BLOX using Lasso, Ridge, SVR and NN-based models.

S2. Regression performance of the RF-based prediction model.

S3. Regression performance of the NN-based prediction model.

S4. Training and selection time of BLOX.

3. Detailed information of test molecules (i)-(viii)

T1. Detailed information of tested molecules.

4. ¹H-NMR spectra of test molecules (i)-(viii)

S5. ¹H-NMR spectrum of (i).

S6. ¹H-NMR spectrum of (ii).

S7. ¹H-NMR spectrum of (iii).

S8. ¹H-NMR spectrum of (iv).

- S9. $^1\text{H-NMR}$ spectrum of (v).
- S10. $^1\text{H-NMR}$ spectrum of (vi).
- S11. $^1\text{H-NMR}$ spectrum of (vii).
- S12. $^1\text{H-NMR}$ spectrum of (viii).

5. Dependence of UV-vis spectra on concentration and solvents

- S13. UV-vis absorption spectra of (i)-(viii) with various concentrations.
- S14. UV-vis absorption spectra of (i)-(viii) with various solvents.
- S15. UV-vis absorption spectra of various solvents.

6. Analyses with HRMS and HPLC

- 6.1 General Experimental Details
- T2. Summary of HRMS results.
- T3. Summary of HPLC data.
- S16. HRMS analysis of (ii).
- S17. HRMS analysis of (iii).
- S18. HRMS analysis of (iv).
- S19. HRMS analysis of (v).
- S20. HRMS analysis of (vi).
- S21. HRMS analysis of (vii).
- S22. HRMS analysis of (viii).
- S23. HPLC analysis of (ii).
- S24. HPLC analysis of (iii).
- S25. HPLC analysis of (iv).
- S26. HPLC analysis of (v).
- S27. HPLC analysis of (vi).
- S28. HPLC analysis of (vii).
- S29. HPLC analysis of (viii).

1 Stein novelty

We calculate *Stein novelty* (SN) using Stein discrepancy to select the most deviated data as follows. For given two distribution p and q , we can measure a distance between them based on kernelized Stein discrepancy as follows,

$$S(p, q) = E_{\mathbf{x}, \mathbf{x}' \sim p}[\delta_{p,q}(\mathbf{x})^T k(\mathbf{x}, \mathbf{x}') \delta_{p,q}(\mathbf{x}')^T], \quad (1)$$

where $\delta_{p,q}(\mathbf{x}) = s_q(\mathbf{x}) - s_p(\mathbf{x})$, s_p is the score function

$$s_p = \nabla_{\mathbf{x}} \log p(\mathbf{x}), \quad (2)$$

and k is a kernel function. When we use the following Gaussian kernel,

$$k(\mathbf{x}, \mathbf{x}') = \exp\left(-\frac{\|\mathbf{x} - \mathbf{x}'\|^2}{2\sigma^2}\right), \quad (3)$$

and q is the uniform distribution, the discrepancy (1) is described as

$$S(p, q) = E_{\mathbf{x}, \mathbf{x}' \sim p}\left[\sum_{t=1}^d \frac{\partial^2}{\partial x_t \partial x'_t} k(\mathbf{x}, \mathbf{x}')\right], \quad (4)$$

where d is the number of the dimension of the distribution. For the evaluated properties $V = \mathbf{v}_1, \dots, \mathbf{v}_n$ by experiment or simulations, we can perform the goodness-of-fit test against the uniform distribution by the following estimate of Stein discrepancy,

$$\hat{S}(V) = \frac{1}{n(n-1)} \sum_{1 \leq i \neq j \leq n} \sum_{t=1}^d \frac{\partial^2}{\partial v_i \partial v'_t} k(\mathbf{v}_i, \mathbf{v}_j). \quad (5)$$

Given a predicted data \mathbf{v}_p , Stein novelty is defined as

$$N(V, \mathbf{v}_p) = \hat{S}(V) - \hat{S}(V \cup \{\mathbf{v}_p\}). \quad (6)$$

This value becomes large when the distribution of the evaluated data V with the predicted data \mathbf{v}_p is closer to the uniform distribution.

When we have a posterior distribution of a predictor $p(\mathbf{v}|\mathbf{z})$ where \mathbf{z} is an input vector of a ML-based prediction model, expected Stein novelty is defined as

$$\phi(\mathbf{z}) = \int N(V, \mathbf{v}) p(\mathbf{v}|\mathbf{z}) d\mathbf{v}. \quad (7)$$

In this study, we used the predicted value of a ML-based regression model as a posterior distribution. We employ $\phi(\mathbf{z})$ as the acquisition function to choose the next candidate, i.e., we calculate $\phi(\mathbf{z})$ for each candidate \mathbf{z} in the unchecked candidates and select the candidate \mathbf{z}' with the highest $\phi(\mathbf{z}')$.

2 Results of BLOX using Lasso, Ridge, SVR, and NN-based models

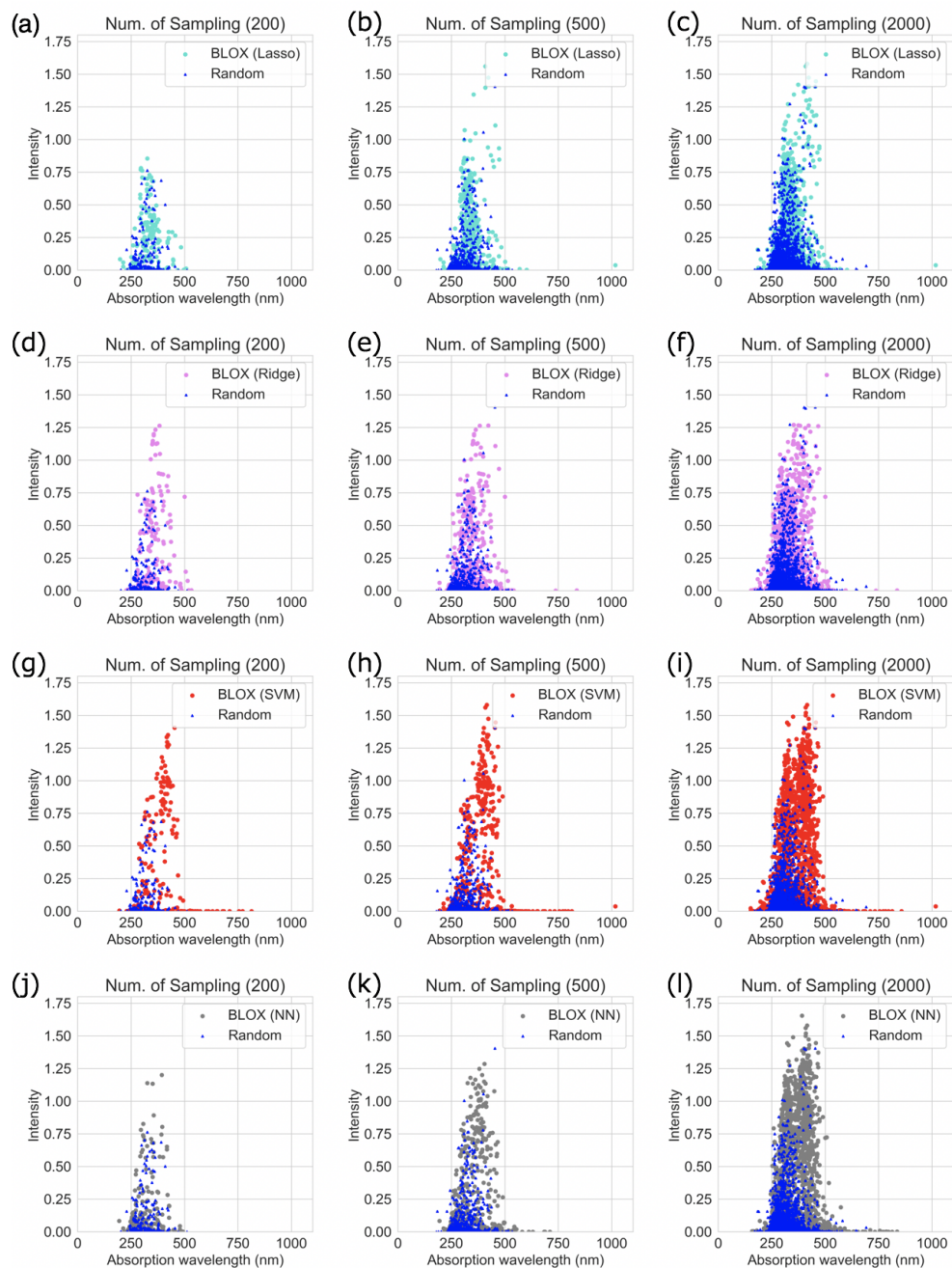


Figure S1: Sampling result of BLOX using the Lasso (a)-(c), Ridge (d)-(f), SVR (g)-(i) and NN (j)-(l) based prediction models. Blue points represent the result of random sampling. All distributions of sampled points by BLOXes are deviated from the trend in the property space. The molecules found by BLOX with SVR are widely distributed, compared to the results by BLOXes with Lasso and Ridge. For BLOX with NN, the distribution was less widespread when the number of samples was small (200 or 500), but the result of the 2000 samplings was relatively wide.

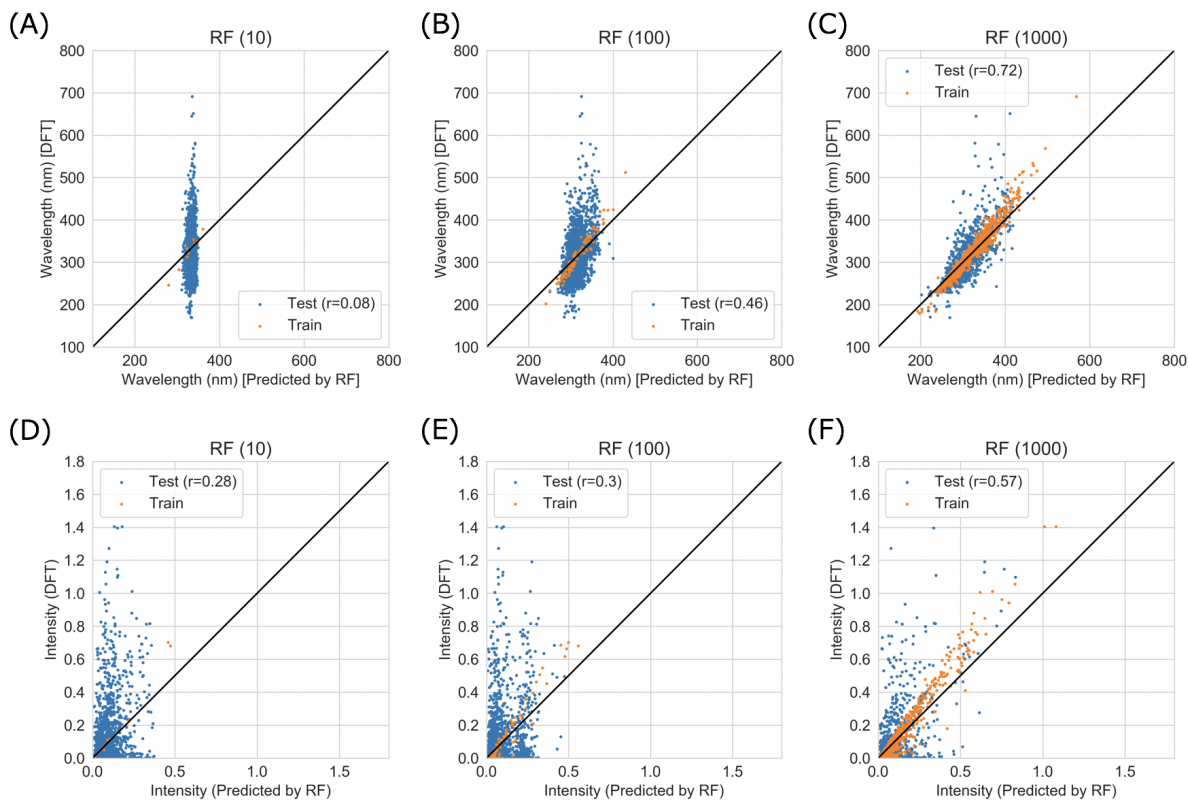


Figure S2: Regression performance of the RF-based prediction models for absorption wavelength (top row) and intensity (bottom row). We used randomly sampled 2000 molecules (blue points in Fig.3(c)). In (A) and (D), the prediction models were trained using only 10 molecules (orange) and prediction performances were tested for the remaining 990 molecules (blue). Each r indicates the correlation coefficient. 100 molecules were used for training in (B) and (E), and 1000 molecules in (C) and (F).

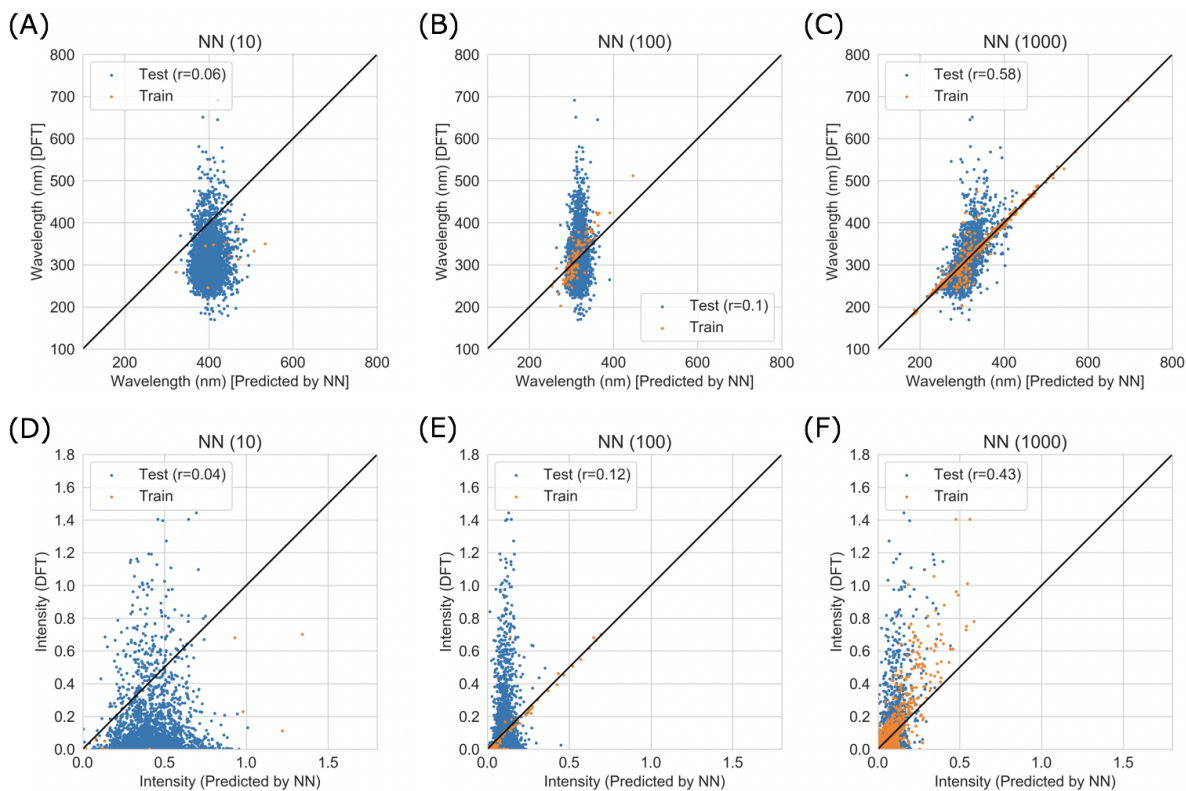


Figure S3: Regression performance of the NN-based prediction models for absorption wavelength (top row) and intensity (bottom row). The setting of training and test is the same as Figure S2. We used randomly sampled 2000 molecules (blue points in Fig.3(c)). In (A) and (D), the prediction models were trained using only 10 molecules (orange) and prediction performances were tested for the remaining 990 molecules (blue). Each r indicates the correlation coefficient. 100 molecules were used for training in (B) and (E), and 1000 molecules in (C) and (F).

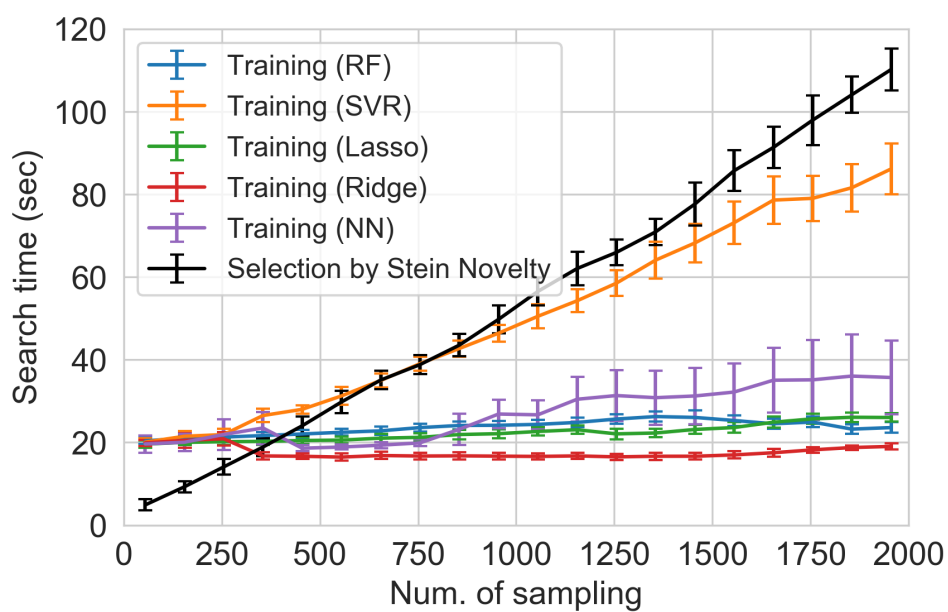


Figure S4: Training and prediction time of the RF (blue), SVR (orange), Lasso (green), Ridge (red), and NN (purple) based prediction models and selection time base on Stein novelty (black). A 12 core (Intel Xeon Gold 6148 CPU) server was used. Although the calculation time tends to increase as the number of observed data increases, the calculation is finished in a few tens of seconds to about 2 minutes.

3 Detailed information of test molecules (i)-(viii)

Table S1: Detailed information of tested molecules (i)-(viii).

Molecule	Name	Supplier	Catalog No.
(i)	1,3,5-Trioxane, 2,4,6-trimethyl-	InterBioScreen Ltd.	BB_SC-07046
(ii)	1-Oxa-3-azaspiro[4.5]decan-2-one, 3-cyclohexyl-4-methylene-	Chemical Block International Ltd.	A1702/0072489
(iii)	1,3,5-Triazin-2-amine, N-[4-(2-benzoxazolyl)phenyl]-4,6-dimethoxy-	Chemical Block International Ltd.	A2930/0123294
(iv)	5(4H)-Oxazolone, 4-[(4- chlorophenyl)methylene]-2-(2-phenylethenyl)-	ChemDiv Inc.	K088-1127
(v)	Benzenamine, 4-(4-morpholinyl)-N-[(5-nitro- 2-thienyl)methylene]-	Enamine Ltd.	Z3226120774
(vi)	Acetamide, N-[4-[(3-chloro-1,4-dihydro-1,4- dioxo-2-naphthalenyl)amino]phenyl]-	ChemDiv Inc.	4204-0009
(vii)	1,4-Naphthalenedione, 2-chloro-3-[(4-methoxyphenyl)amino]-	ChemDiv Inc.	4204-0007
(viii)	1,4-Naphthalenedione, 2-chloro-3-[[4-(dimethylamino)phenyl]amino]-	Enamine Ltd.	Z2065672195

4 $^1\text{H-NMR}$ spectra of test molecules (i)-(viii)

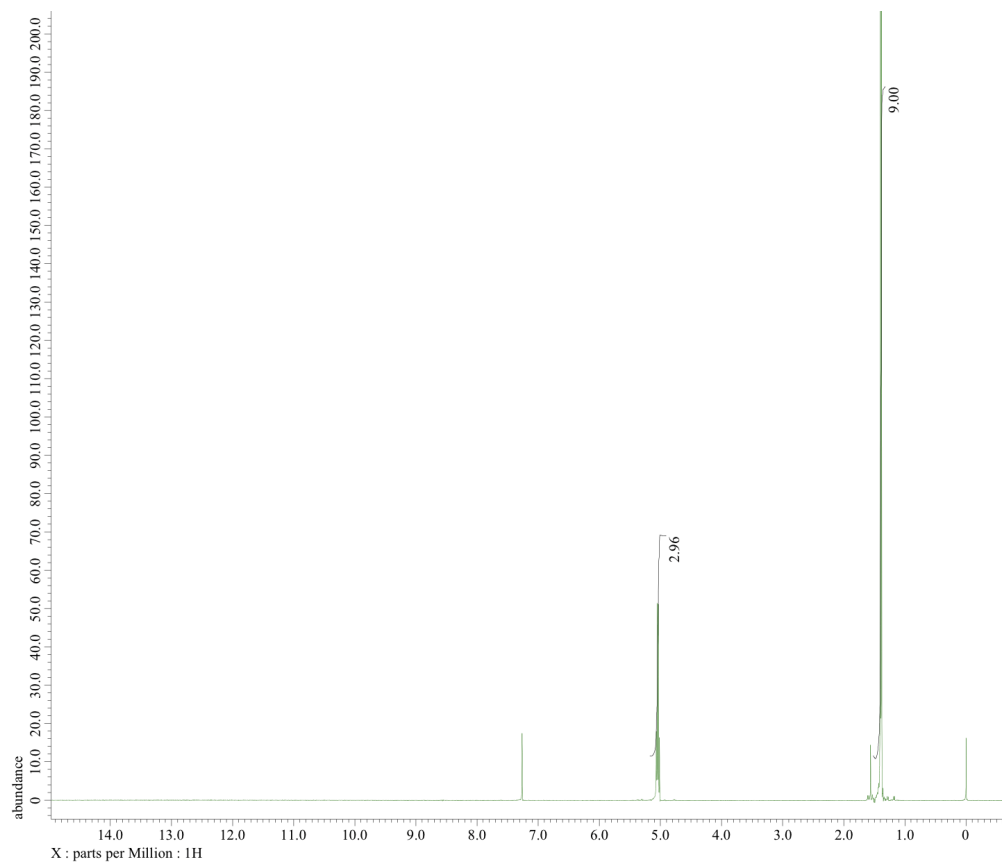


Figure S5: $^1\text{H-NMR}$ spectrum of (i). $^1\text{H-NMR}$ (300 MHz, CDCl_3 , 22 $^\circ\text{C}$) in ppm: 5.04 (q, $J = 5.1$ Hz, CH), 1.39 (d, $J = 5.1$ Hz, CH_3).

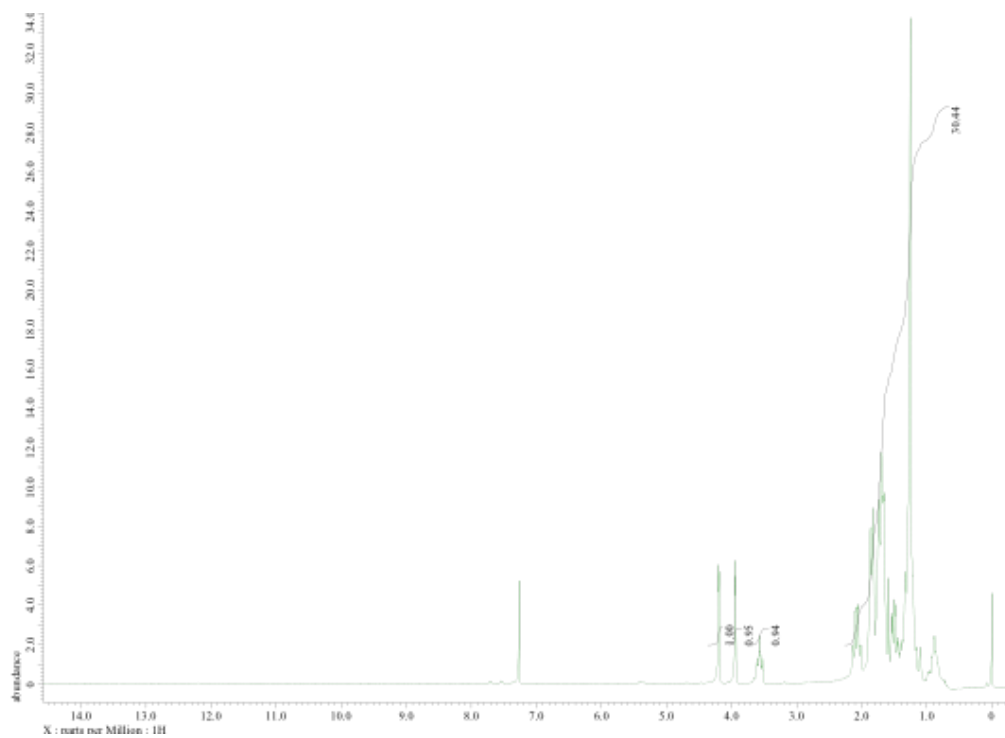


Figure S6: ¹H-NMR spectrum of (ii). The material was purified by column chromatography on silica gel (eluent: dichloromethane/hexane = 1/1). ¹H-NMR (300 MHz, CDCl₃, 23 °C) in ppm: 4.20 (d, $J = 3.0$ Hz, 1H, C=CH₂), 3.94 (d, $J = 2.7$ Hz, 1H, C=CH₂), 3.57 (m, 1H, CH), 2.1-0.9 (m, 30H, CH₂ and H₂O).

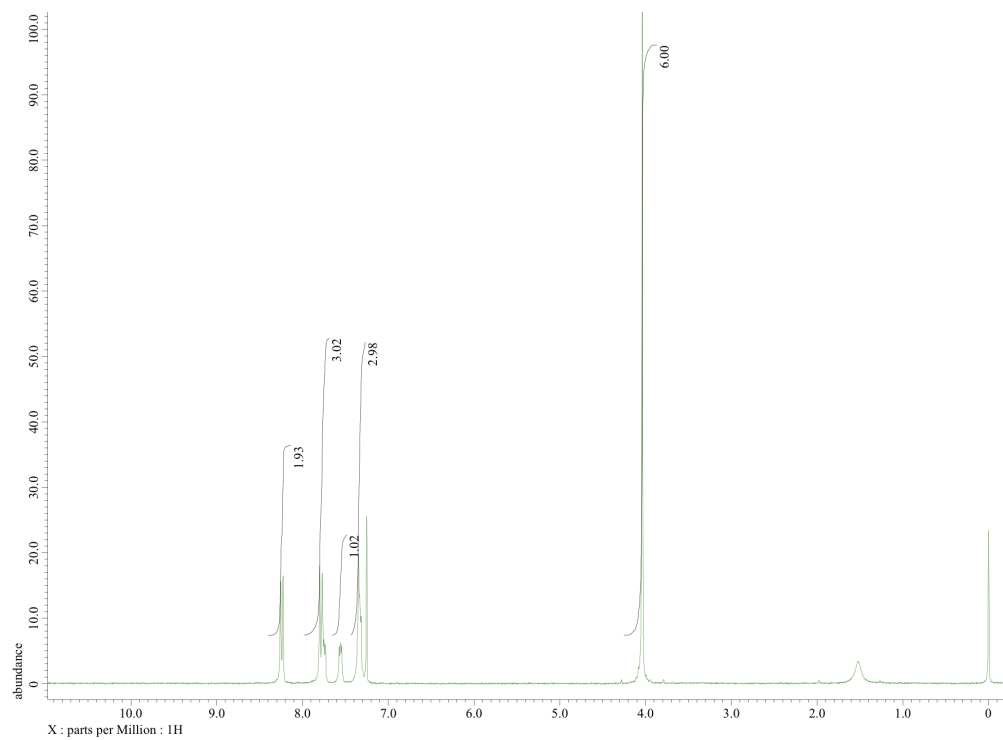


Figure S7: ¹H-NMR spectrum of (iii). ¹H-NMR (300 MHz, CDCl₃, 50 °C) in ppm: 8.24 (d, *J* = 8.4 Hz, 2H, ArH), 7.78 (d, *J* = 9.0 Hz, 2H, ArH), 7.75 (m, 1H, ArH), 7.56 (m, 1H, ArH), 7.35 (m, 3H, ArH and NH), 4.04 (s, 6H, CH₃).

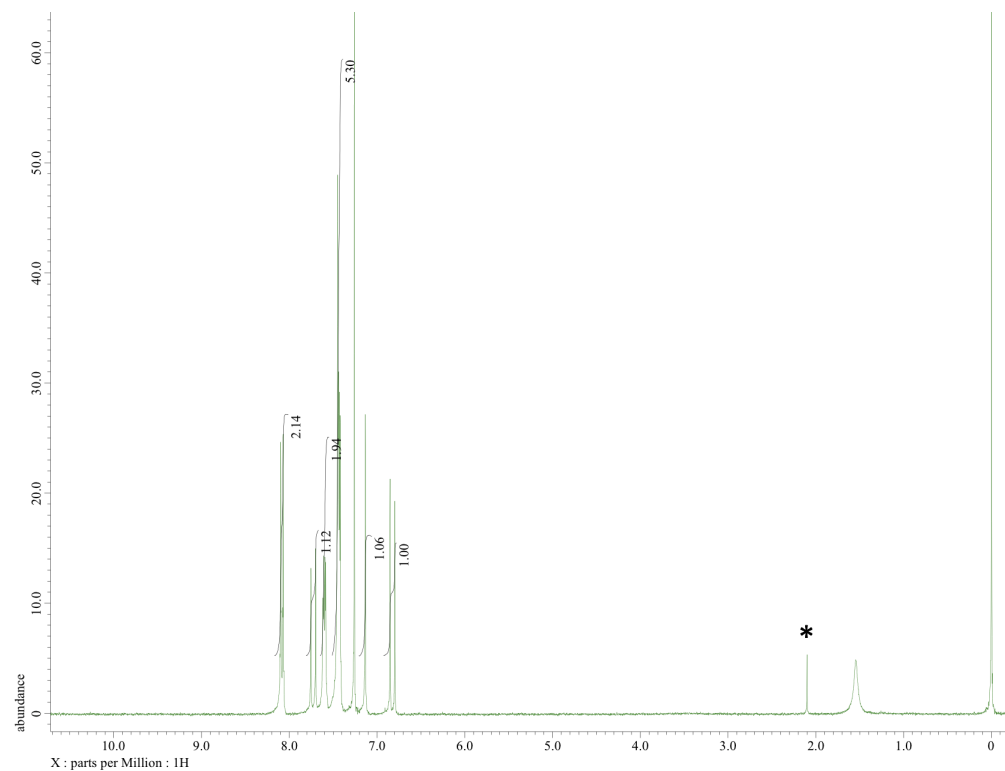


Figure S8: ¹H-NMR spectrum of (iv). ¹H-NMR (300 MHz, CDCl₃, 23 °C) in ppm: 8.08 (d, $J = 9.0$ Hz, 1H, ArH), 7.73 (d, $J = 16.2$ Hz, 1H, CH=CH), 7.59 (m, 2H, ArH), 7.43 (m, 5H, ArH), 7.13 (s, 1H, C=CH), 6.82 (d, $J = 16.2$ Hz, 1H, CH=CH). Asterisk denotes a solvent signal.

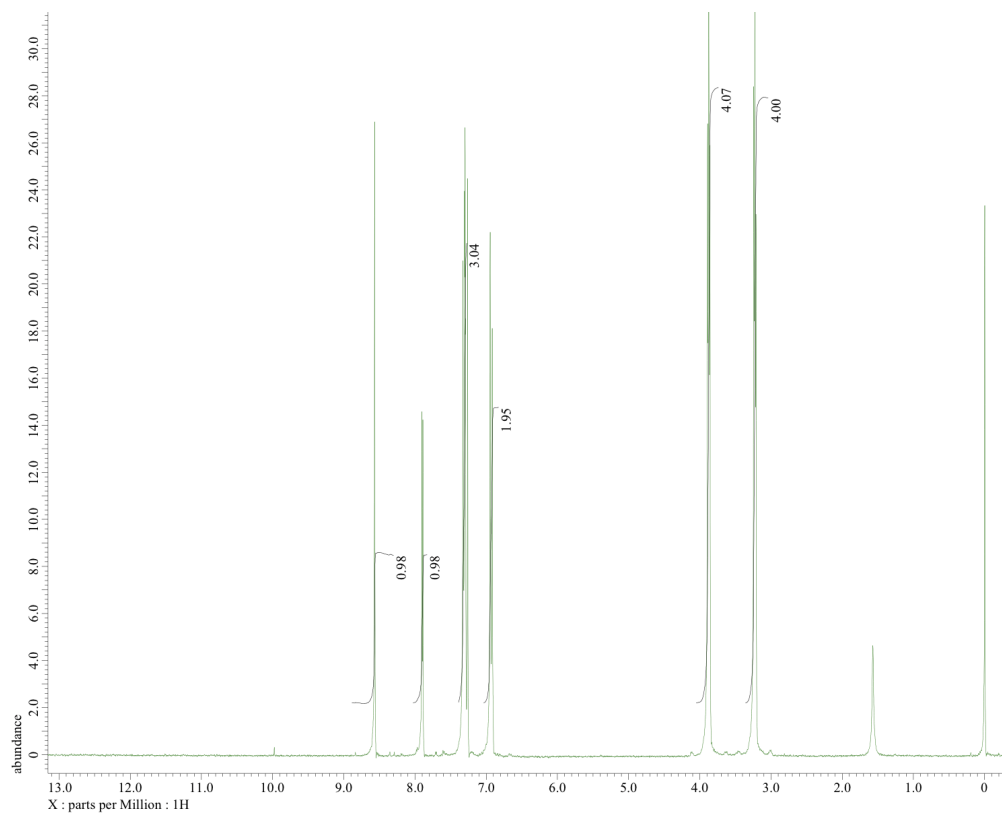


Figure S9: ^1H -NMR spectrum of (v). ^1H -NMR (300 MHz, CDCl_3 , 20 $^\circ\text{C}$) in ppm: 8.57 (s, 1H, N=CH), 7.90 (d, $J = 4.5$ Hz, 1H, ArH), 7.32-7.30 (m, 3H, ArH), 6.93 (d, $J = 8.7$ Hz, 2H, ArH), 3.88 (t, $J = 4.5$ Hz, 4H, CH_2), 3.23 (t, $J = 4.8$ Hz, 4H, CH_2).

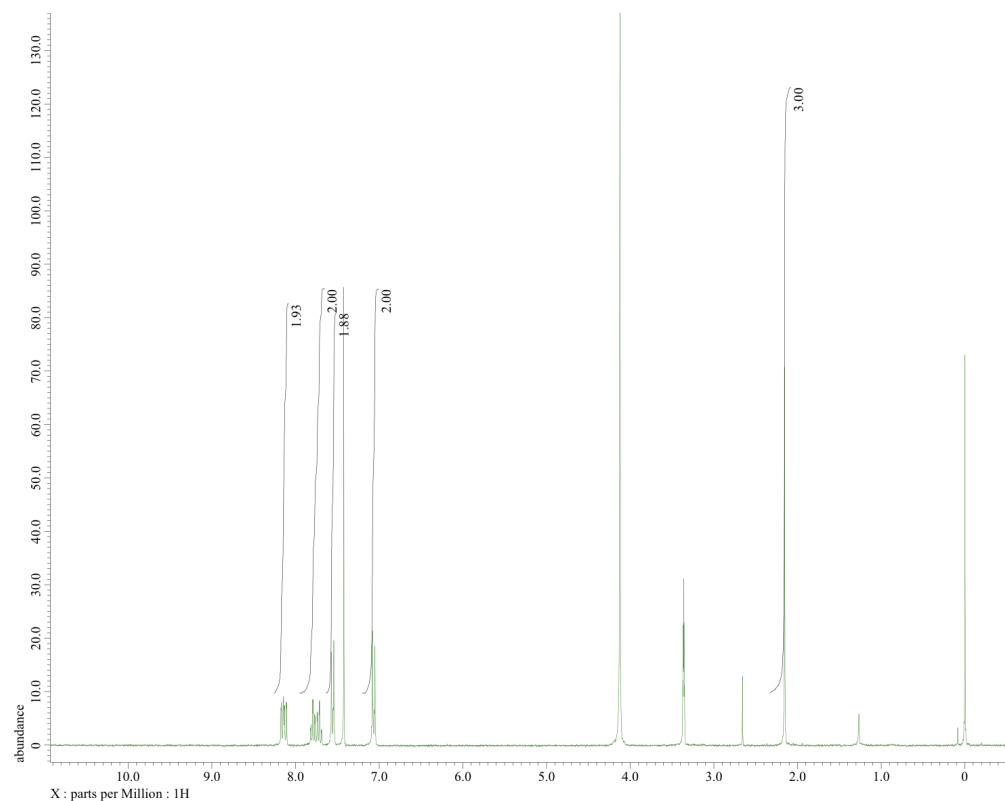


Figure S10: ¹H-NMR spectrum of (vi). ¹H-NMR (300 MHz, CDCl₃/CD₃OD = 4/1 in vol., 22 °C) in ppm: 8.16 (dd, *J* = 7.5 and 0.9 Hz, 1H, ArH), 8.12 (dd, *J* = 7.8 and 1.5 Hz, 1H, ArH), 7.79 (td, *J* = 7.5 and 1.5 Hz, 1H, ArH), 7.71 (td, *J* = 7.5 and 1.5 Hz, 1H, ArH), 7.56 (d, *J* = 8.7 Hz, 2H, ArH), 7.07 (d, *J* = 9.0 Hz, 2H, ArH), 2.16 (s, 1H, CH₃).

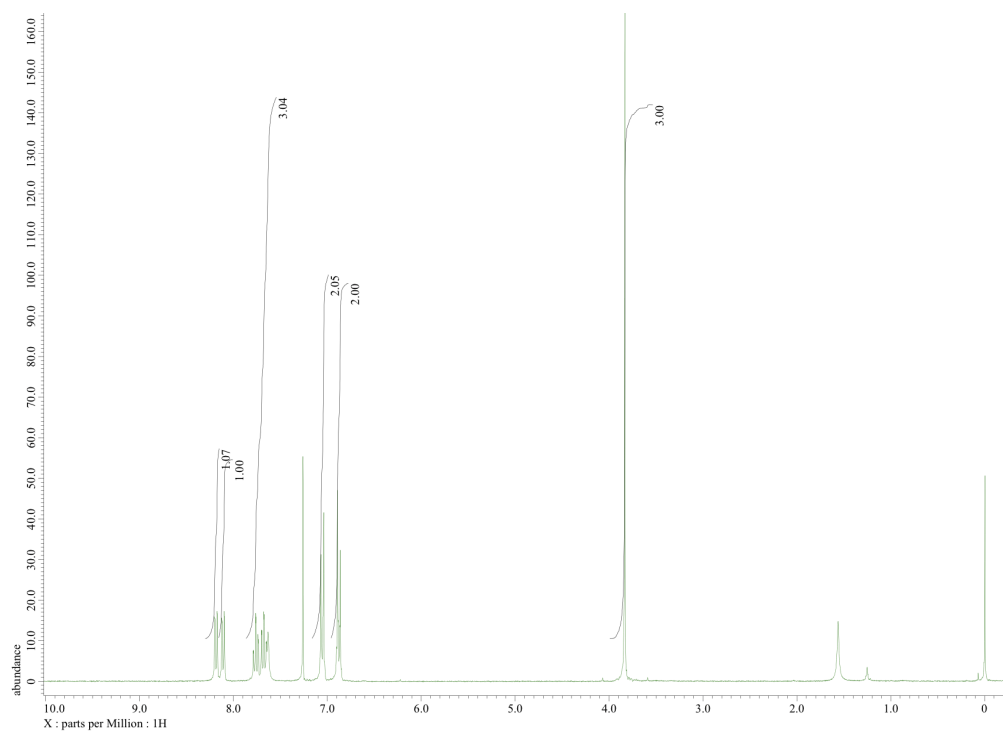


Figure S11: ¹H-NMR spectrum of (vii). ¹H-NMR (300 MHz, CDCl₃, 22 °C) in ppm: 8.18 (dd, $J = 7.8$ and 0.9 Hz, 1H, ArH), 8.11 (dd, $J = 7.5$ and 0.9 Hz, 1H, ArH), 7.76 (td, 1H, $J = 7.5$ and 0.9 Hz, ArH), 7.67 (td, $J = 7.5$ and 0.9 Hz, 1H, ArH), 7.63 (br, 1H, NH), 7.05 (d, $J = 8.7$ Hz, 2H, ArH), 6.88 (d, 2H, $J = 8.7$ Hz, ArH), 3.83 (s, 3H, CH₃).

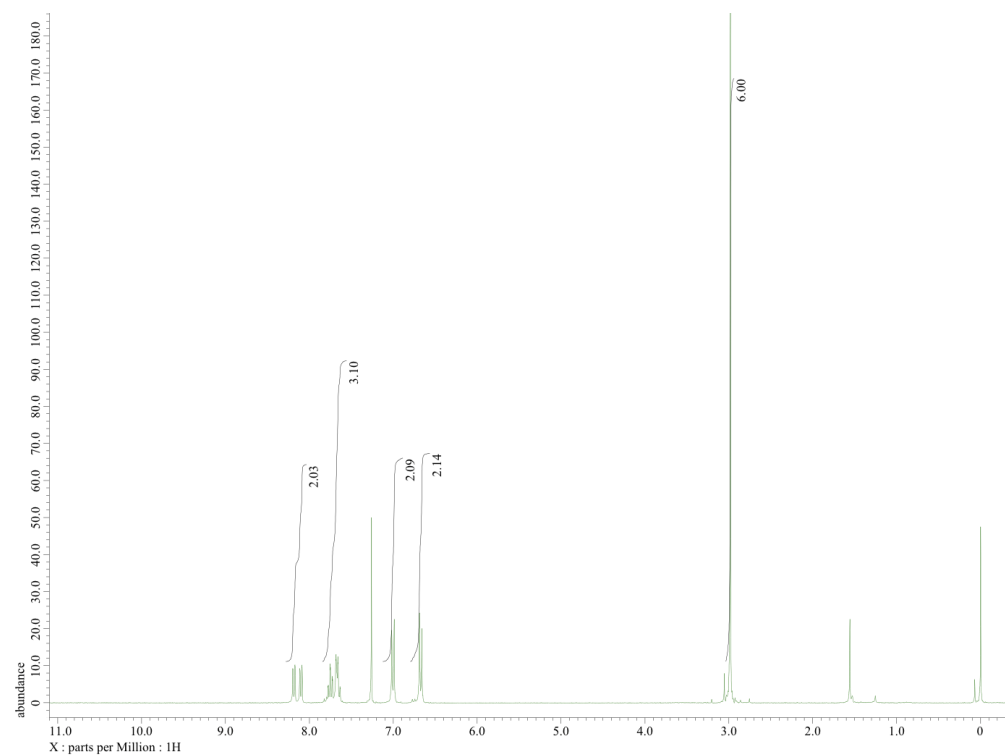


Figure S12: ¹H-NMR spectrum of (viii). ¹H-NMR (300 MHz, CDCl₃, 20 °C) in ppm: 8.19 (d, $J = 7.8$ Hz, 1H, ArH), 8.10 (d, $J = 8.4$ Hz, 1H, ArH), 7.75 (td, $J = 7.2$ and 1.2 Hz, 1H, ArH), 7.69-7.63 (m, 2H, ArH and NH), 7.00 (d, $J = 8.7$ Hz, 2H, ArH), 6.67 (d, $J = 9.0$ Hz, 2H, ArH), 2.98 (s, 6H, CH₃).

5 Dependence of UV-vis spectra on concentration and solvents

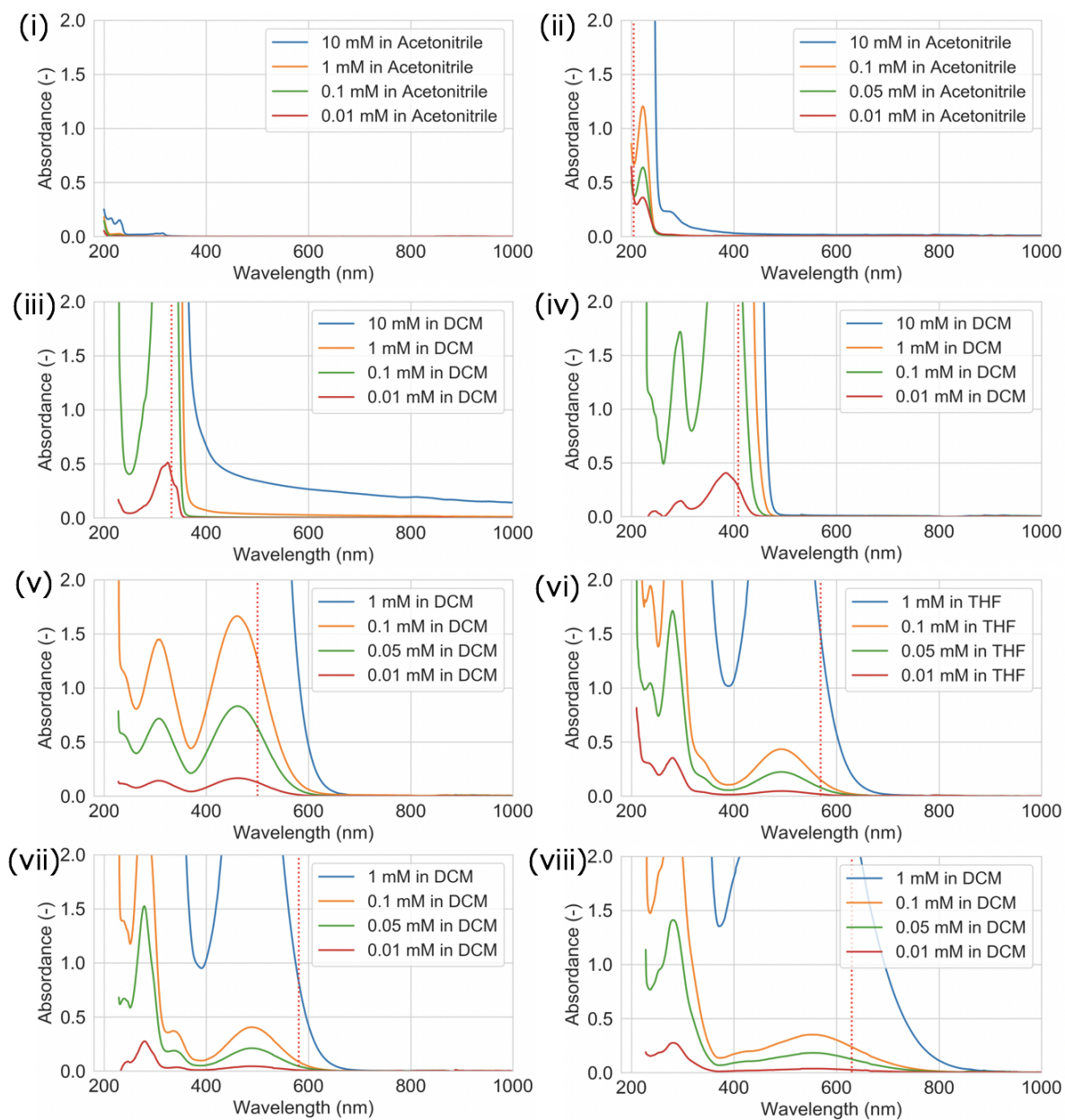


Figure S13: Experimental UV-vis absorption spectra of (i)-(viii) with various concentration.

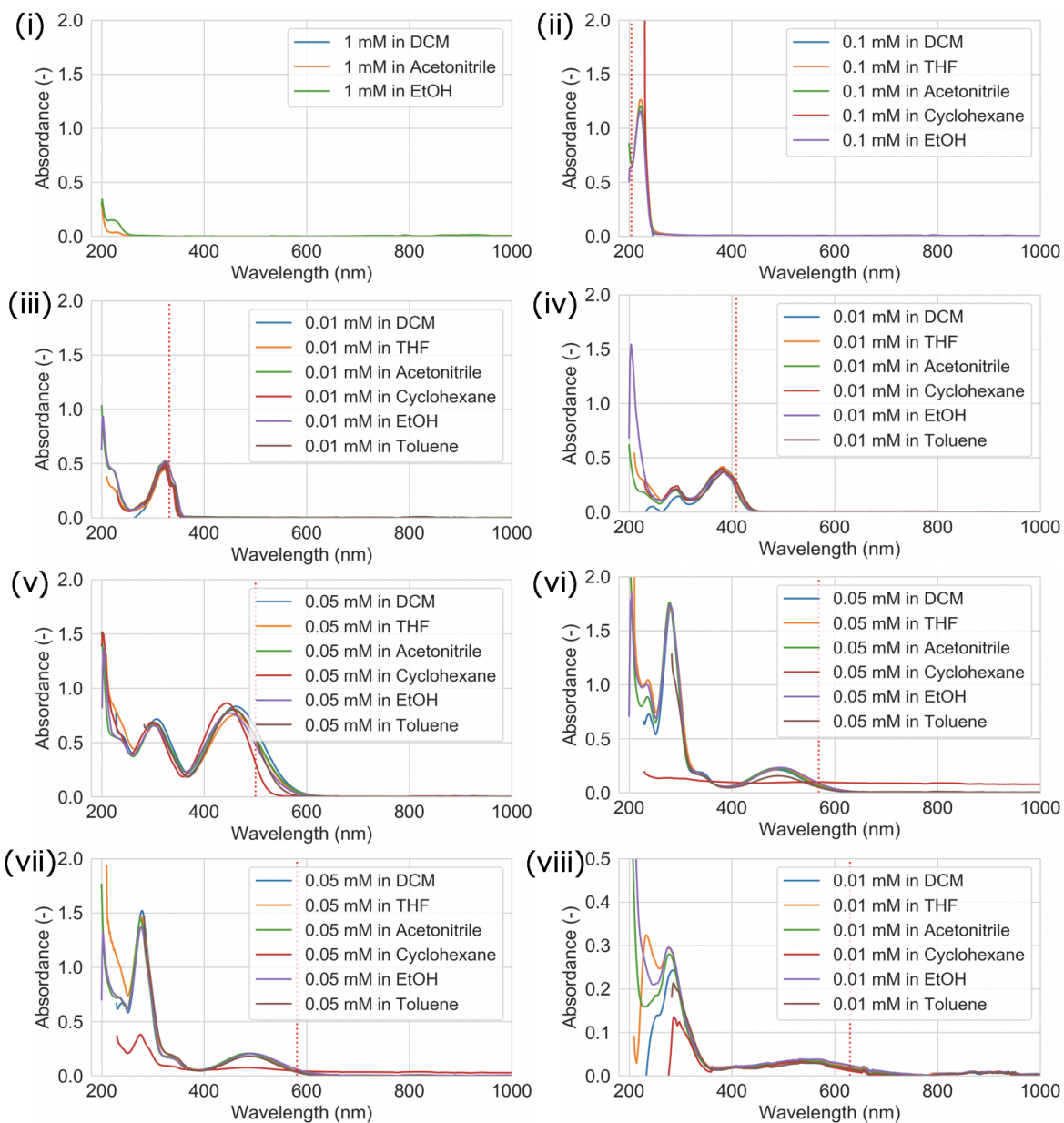


Figure S14: Experimental UV-vis absorption spectra of (i)-(viii) in various solvent.

6 Analyses with HRMS and HPLC

6.1 General Experimental Details

High resolution mass spectrometry was recorded on a Bruker TIMS-TOF spectrometer with samples dissolved in 1:1 acetonitrile:methanol (0.1 mg/mL).

HPLC data was recorded on a JASCO extrema with modules CO-4061, AS-4050, MD-4010 and 2 × PU-4086 utilising HPLC grade solvents as eluent. All samples were dissolved in acetonitrile (0.5 mg/mL) and one of the following three methods was utilised with a TOSOH TSKgel ODS-80Ts 4.6 mm ID × 15 cm L HPLC column equipped with the recommended pre-column guard.

10-100% MeOH in H₂O

Injection volume: 50 μL

Column oven temperature: 30 °C

Flow rate: 0.8 mL/min

Acquisition time: 60 mins

Gradient profile: 0 - 5 min = 10% MeOH, 5 - 45 min = 10-100% MeOH, 45-50 min = 100% MeOH, 50 - 60 min = 10% MeOH.

50-100% MeOH in H₂O

Injection volume: 50 μL

Column oven temperature: 30 °C

Flow rate: 0.8 mL/min

Acquisition time: 60 mins

Gradient profile: 0 - 5 min = 50% MeOH, 5 - 45 min = 50-100% MeOH, 45-50 min = 100% MeOH, 50 - 60 min = 50% MeOH.

75-100% MeOH in H₂O

Injection volume: 50 μL

Column oven temperature: 30 °C

Flow rate: 0.8 mL/min

Acquisition time: 60 mins

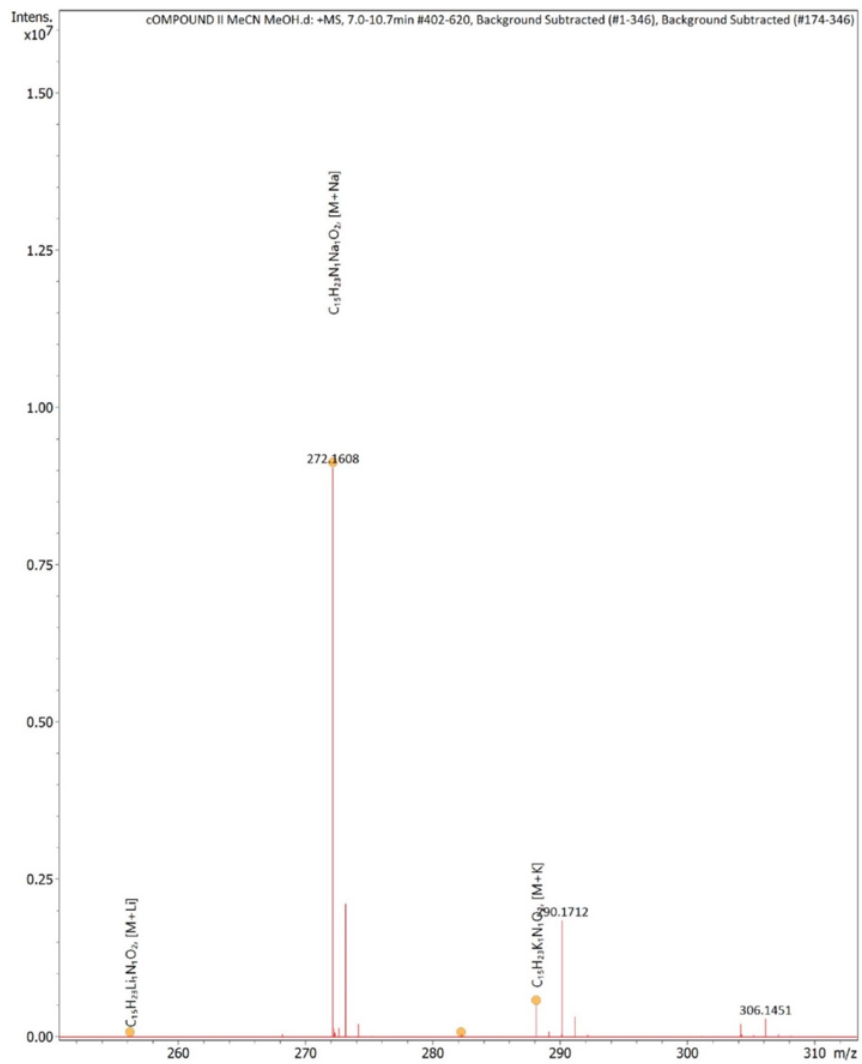
Gradient profile: 0 - 5 min = 75% MeOH, 5 - 45 min = 75-100% MeOH, 45-50 min = 100% MeOH, 50 - 60 min = 75% MeOH.

Table S2: Summary of HRMS result.

Molecule	Molecular Formula	Observed Ion	Theoretical Mass	Observed Mass	Error (ppm)
(ii)	C ₁₅ H ₂₃ NO ₂	[M+Na] ⁺	272.1621	272.1608	4.7
(iii)	C ₁₈ H ₁₅ N ₅ O ₃	[M+H] ⁺	350.1248	350.1246	0.4
(iv)	C ₁₈ H ₁₂ ClNO ₂	[M+MeOH-H] ⁻	340.0746	340.0722	6.9
(v)	C ₁₅ H ₁₅ N ₃ O ₃ S	[M+H] ⁺	318.0906	318.0891	5.1
(vi)	C ₁₈ H ₁₃ ClN ₂ O ₃	[M+H] ⁺	341.0687	341.0674	4.1
(vii)	C ₁₇ H ₁₂ ClNO ₃	[M+H] ⁺	314.0578	314.0567	3.6
(viii)	C ₁₈ H ₁₅ ClN ₂ O ₂	[M+H] ⁺	327.0895	327.0882	4.0

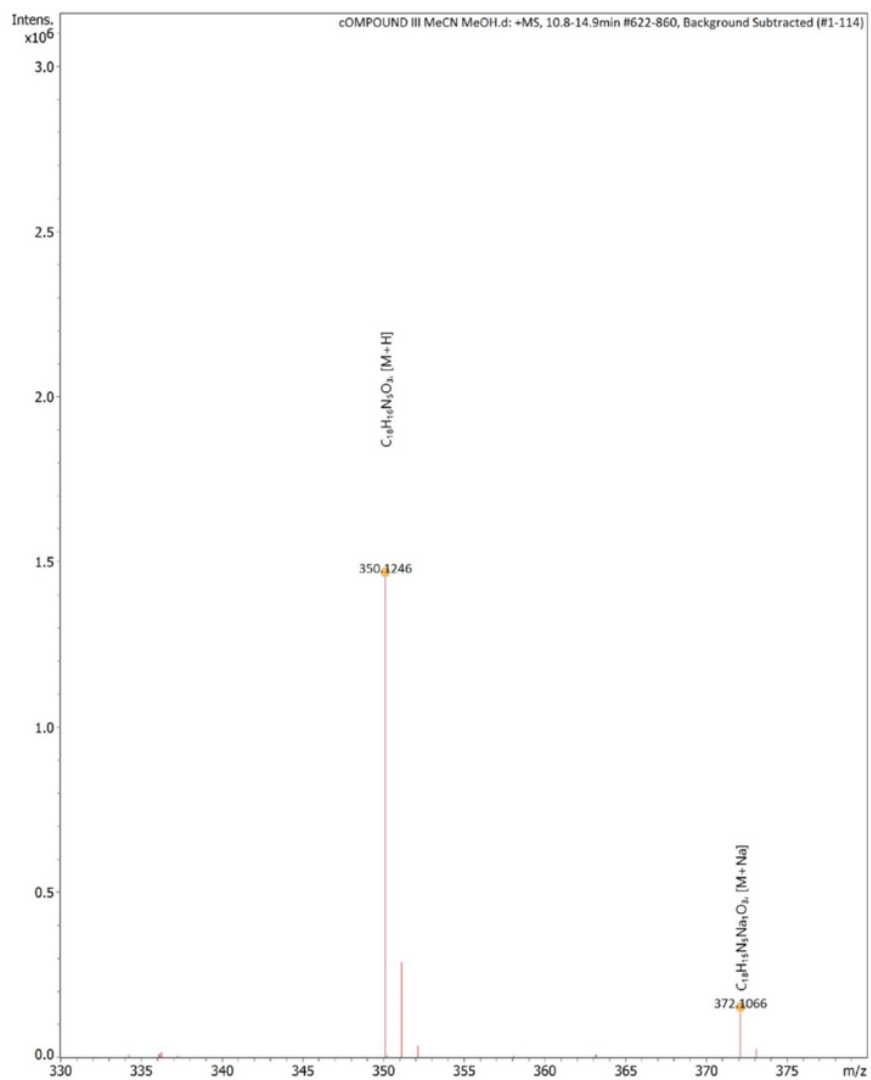
Table S3: Summary of HPLC data.

Molecule	Method	Retention time (min)	Purity
(ii)	50-100% MeOH in H ₂ O	29.6	>99.5%
(iii)	10-100% MeOH in H ₂ O	42.9	98.8%
(iv)	75-100% MeOH in H ₂ O	21.3	99.9%
(v)	10-100% MeOH in H ₂ O	40.8	99.0%
(vi)	10-100% MeOH in H ₂ O	37.0	96.1%
(vii)	50-100% MeOH in H ₂ O	25.7	97.6%
(viii)	50-100% MeOH in H ₂ O	27.5	92.4%



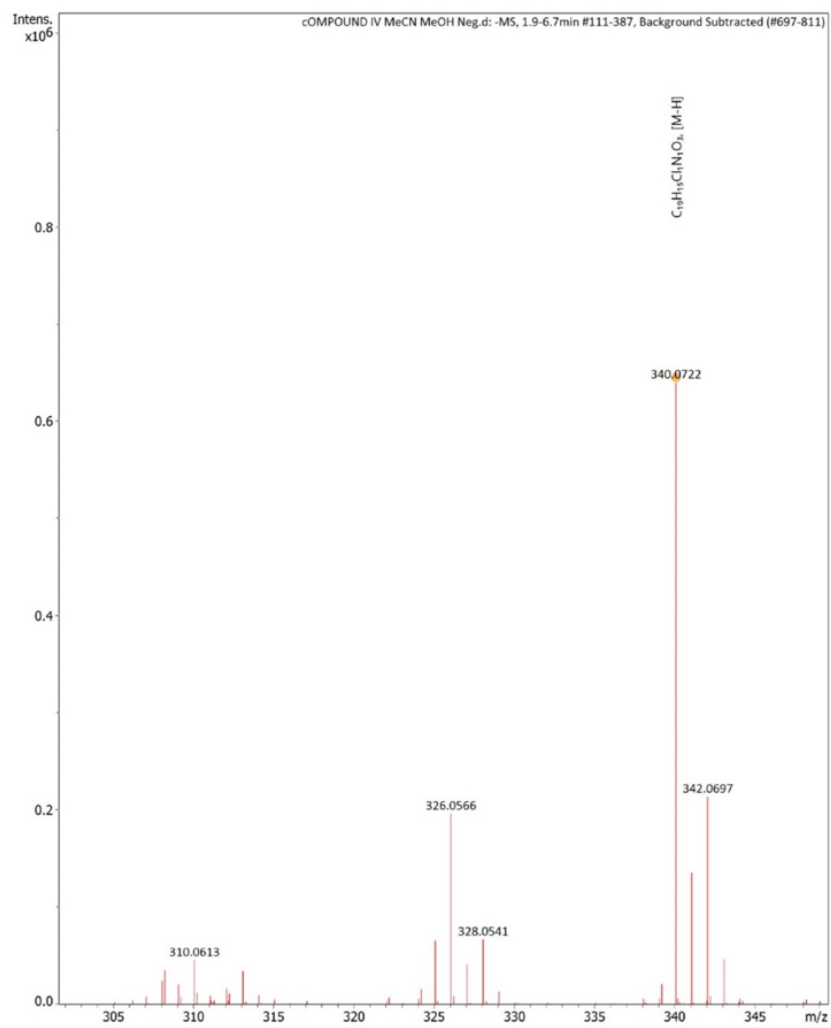
	z	m/z	I	err [mDa]	err [ppm]	mSigma
[M+Na]	1	272.1608	9053610	1.3	4.7	37.3
[M+K]	1	288.1346	505713	1.5	5.1	6

Figure S15: HRMS analysis of molecule (ii).



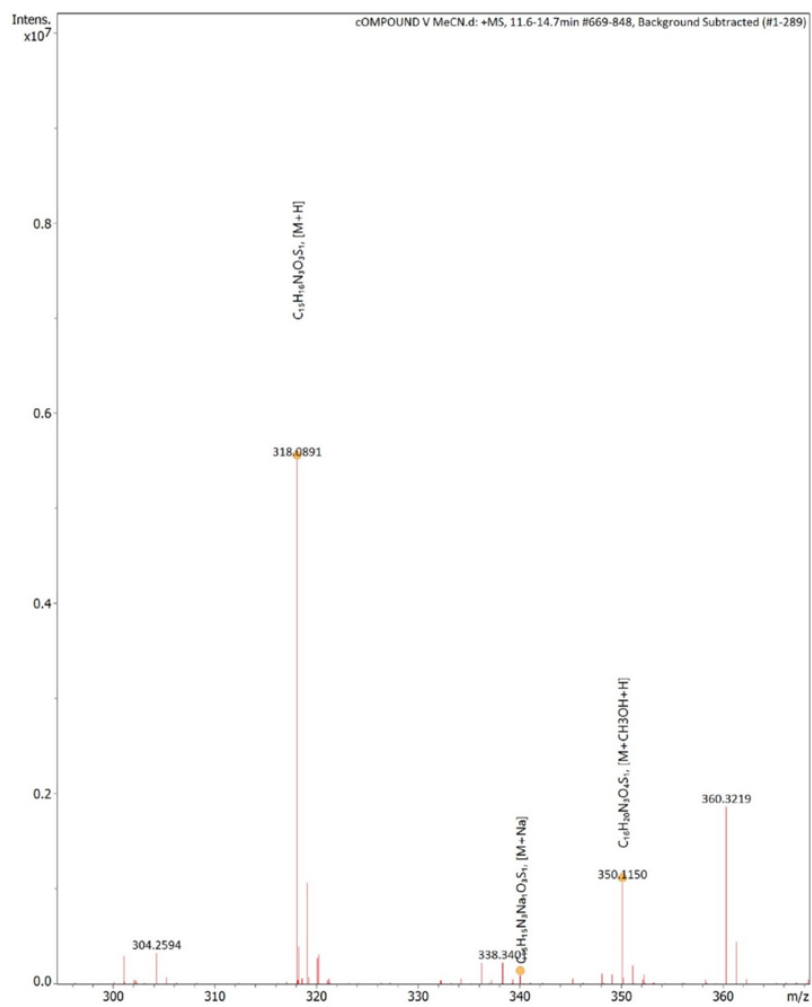
	z	m/z	I	err [mDa]	err [ppm]	mSigma
[M+H]	1	350.1246	1454170	0.1	0.4	9.9
[M+Na]	1	372.1066	138554	0.1	0.2	11

Figure S16: HRMS analysis of molecule (iii).



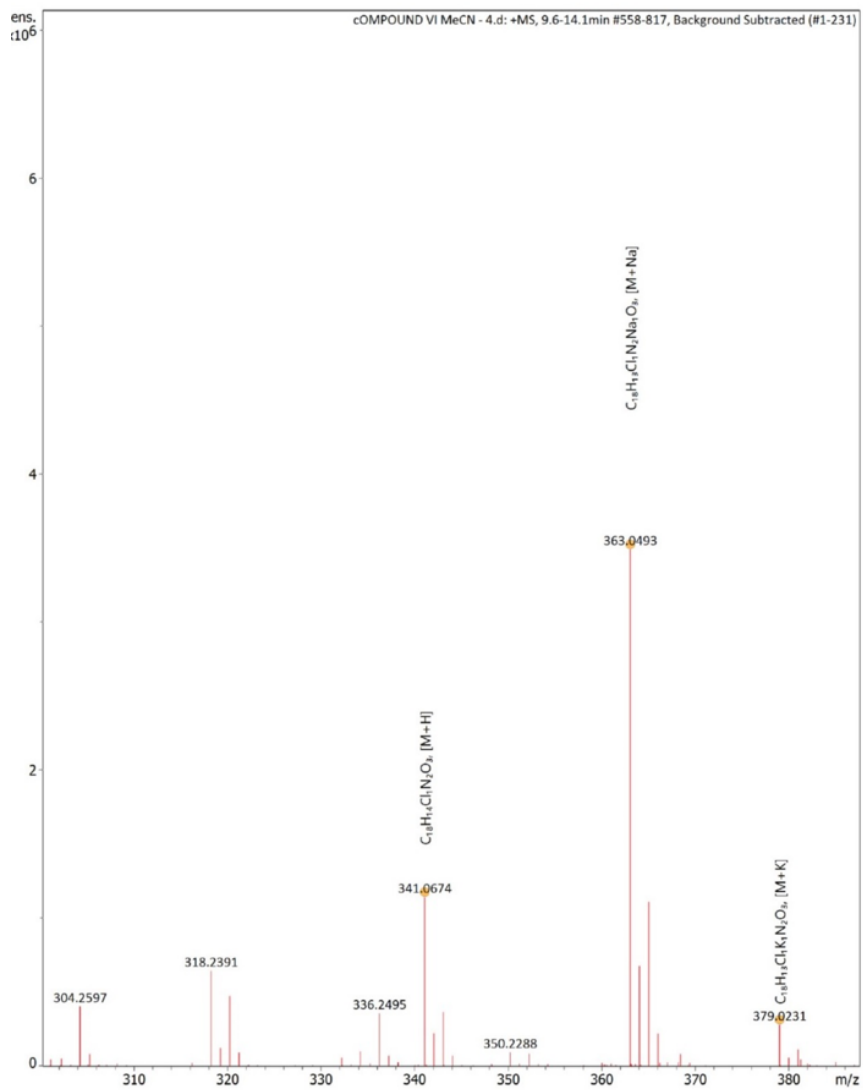
	z	m/z	I	err [mDa]	err [ppm]	mSigma
[M+MeOH-H]	-1	340.0722	639889	2.4	6.9	5.8
[M+MeOH+Cl]	-1	376.0485	14157	2.7	7.3	18.3

Figure S17: HRMS analysis of molecule (iv).



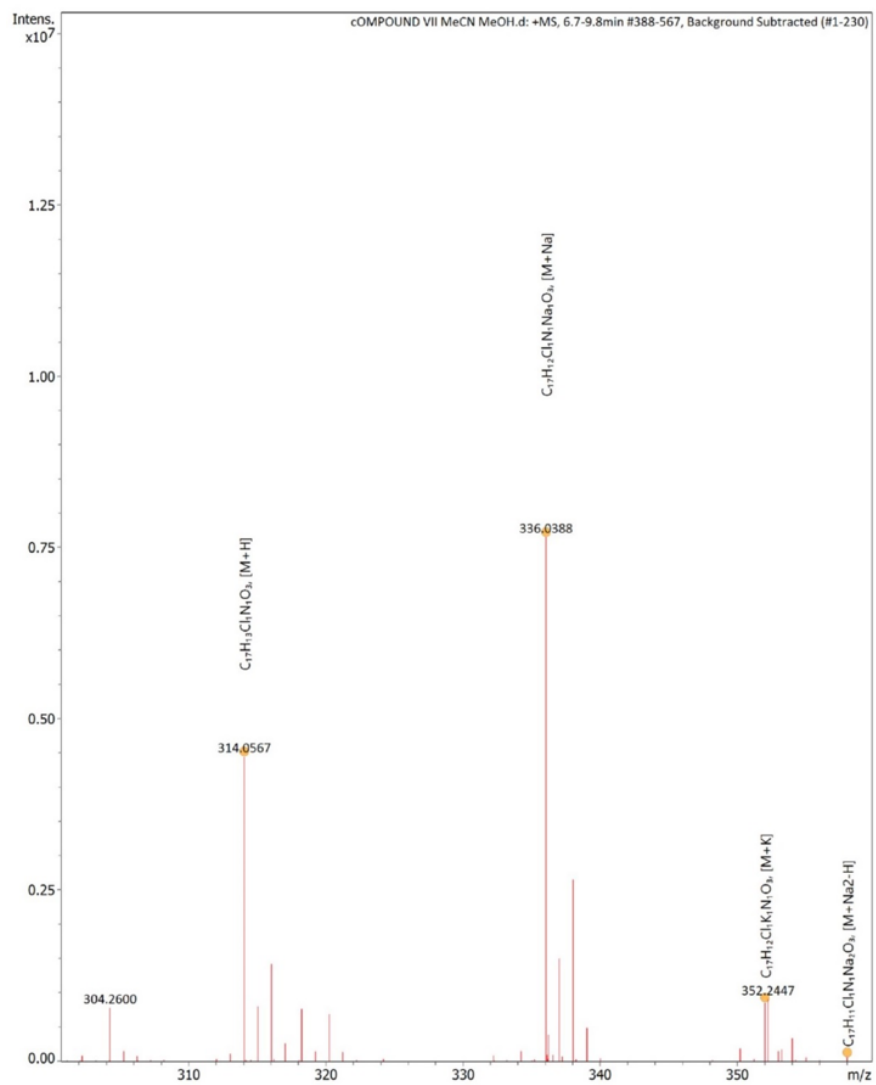
	z	m/z	I	err [mDa]	err [ppm]	mSigma
[M+H]	1	318.0891	5510104	1.6	5.1	9.9
[M+Na]	1	340.0712	96382	1.4	4.2	16.2
[M+CH3OH+H]	1	350.115	1069164	1.9	5.4	12.3

Figure S18: HRMS analysis of molecule (v).



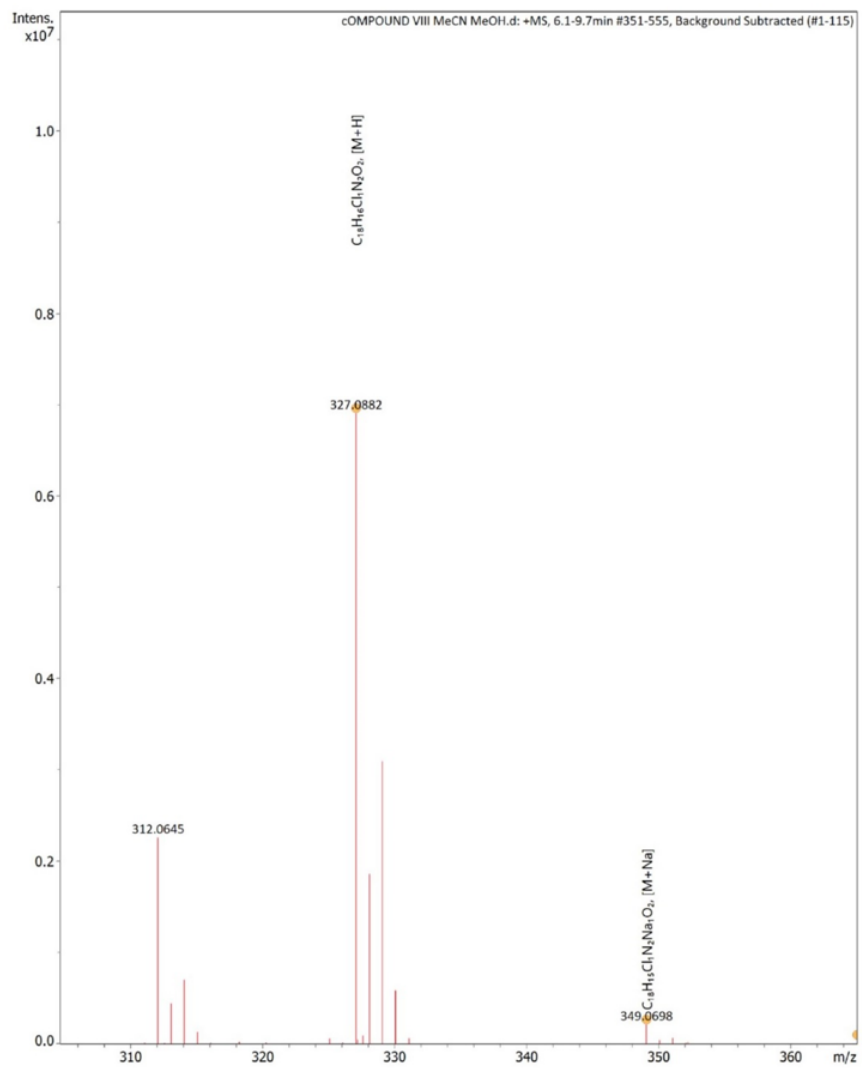
	z	m/z	I	err [mDa]	err [ppm]	mSigma
[M+H]	1	341.0674	1143912	1.4	4.1	12
[M+Na]	1	363.0493	3491562	1.4	3.9	13.1
[M+K]	1	379.0231	282465	1.6	4.1	5

Figure S19: HRMS analysis of molecule (vi).



	z	m/z	I	err [mDa]	err [ppm]	mSigma
[M+H]	1	314.0567	4452063	1.1	3.6	10.9
[M+Na]	1	336.0388	7652644	1	3	3.8
[M+K]	1	352.0126	864708	1.2	3.3	8.1

Figure S20: HRMS analysis of molecule (vii).



	z	m/z	I	err [mDa]	err [ppm]	mSigma
[M+H]	1	327.0882	6909640	1.3	4	55.5
[M+Na]	1	349.0698	217425	1.6	4.5	10

Figure S21: HRMS analysis of molecule (viii).

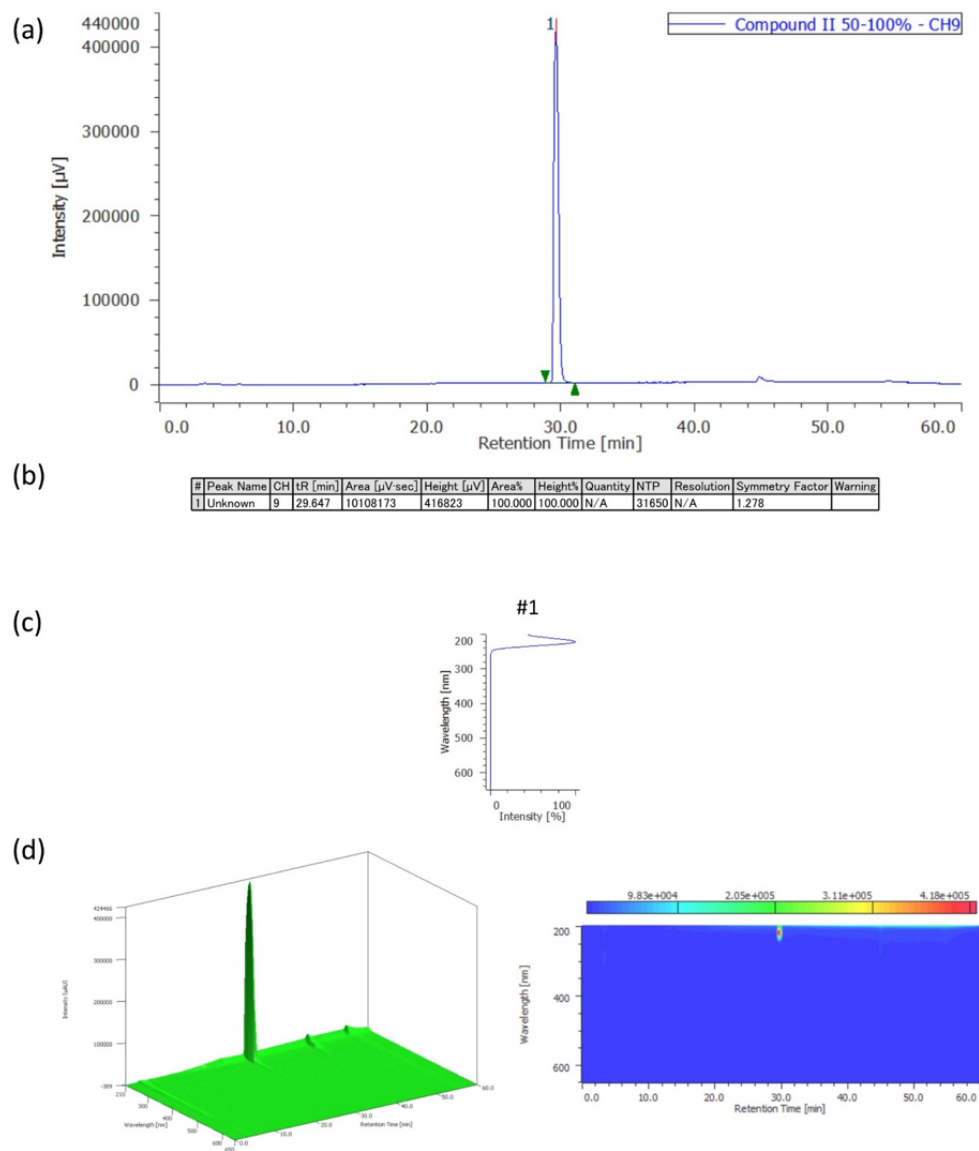
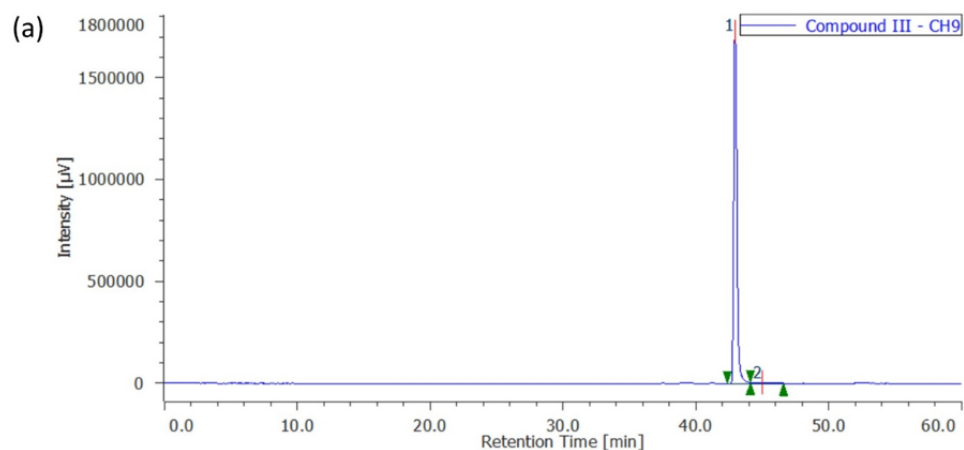


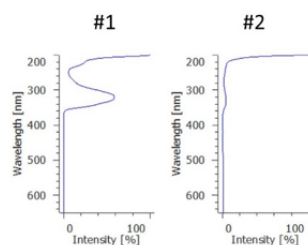
Figure S22: HPLC analysis of molecule (ii) utilising method 50-100% MeOH in H₂O. (a) HPLC trace with detection at 220 nm. (b) Analysis of peak area of compounds detected in sample ii at 220 nm. Signal at 45 min was not include due to its occurrence in the blank sample. (c) Extraction of UV-vis spectra of peak 1 from PDA data. (d) PDA detector data from 200-650 nm shown in 2D and 3D representations.



(b)

#	Peak Name	CH	tR [min]	Area [µV·sec]	Height [µV]	Area%	Height%	Quantity	NTP	Resolution	Symmetry Factor	Warning
1	Unknown	9	42.940	29618421	1724781	98.846	99.749	N/A	153845	N/A	1.396	
2	Unknown	9	45.023	345833	4338	1.154	0.251	N/A	N/A	N/A	N/A	

(c)



(d)

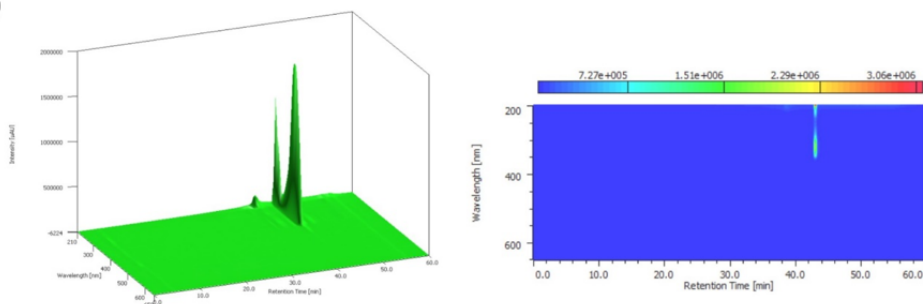


Figure S23: HPLC analysis of molecule (iii) utilising method 10-100% MeOH in H₂O. (a) HPLC trace with detection at 320 nm. (b) Analysis of peak area of compounds detected in sample iii at 320 nm. (c) Extraction of UV-vis spectra of peaks 1-2 from PDA data. (d) PDA detector data from 200-650 nm shown in 2D and 3D representations.

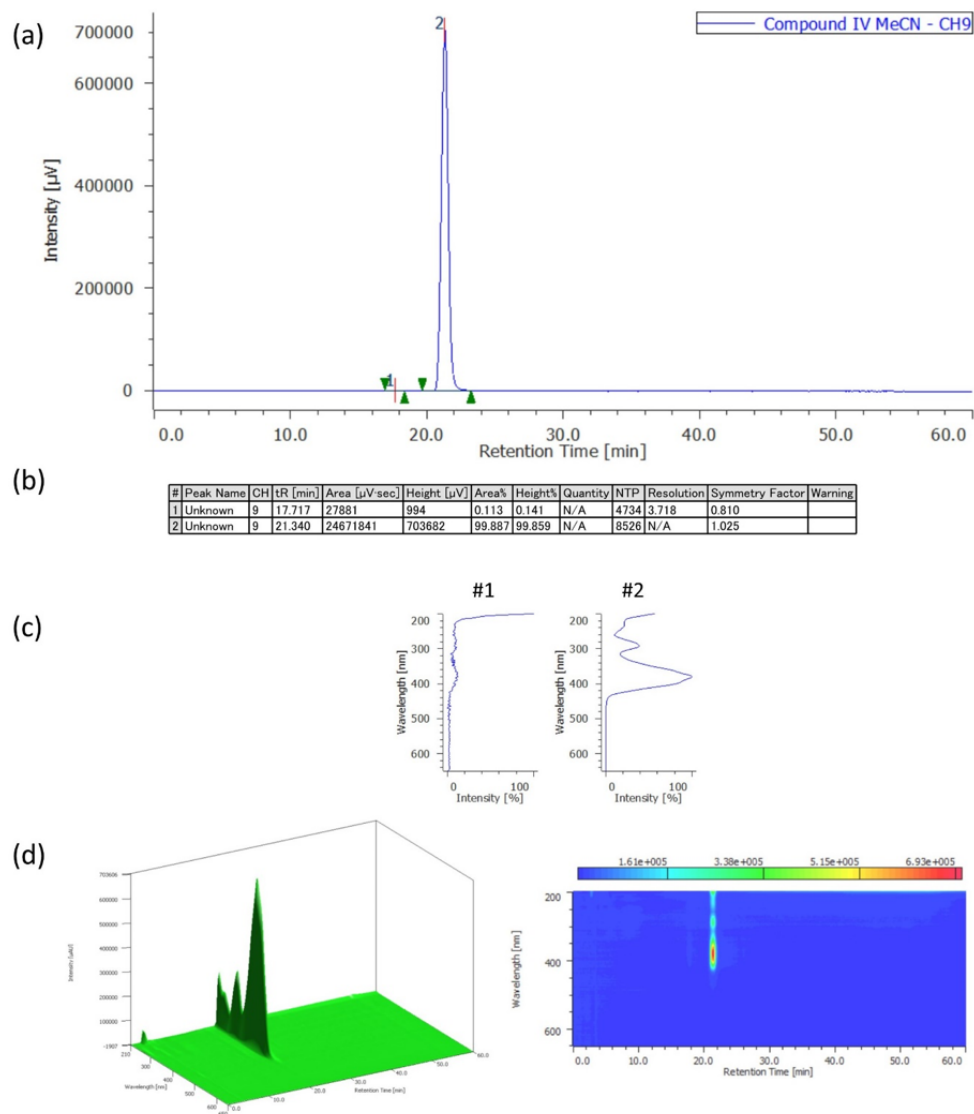
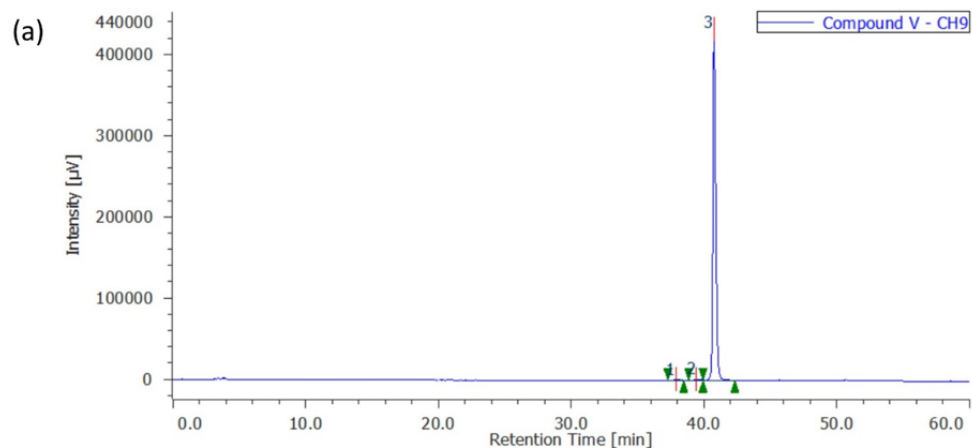


Figure S24: HPLC analysis of molecule (iv) utilising method 75-100% MeOH in H₂O. (a) HPLC trace with detection at 380 nm. (b) Analysis of peak area of compounds detected in sample iv at 380 nm. (c) Extraction of UV-vis spectra of peaks 1-2 from PDA data. (d) PDA detector data from 200-650 nm shown in 2D and 3D representations.



(b) Analysis of peak area of compounds detected in sample v at 450 nm.

#	Peak Name	CH	tR [min]	Area [$\mu\text{V}\cdot\text{sec}$]	Height [μV]	Area%	Height%	Quantity	NTP	Resolution	Symmetry Factor	Warning
1	Unknown	9	37.903	30951	1397	0.473	0.321	N/A	51498	2.472	1.006	
2	Unknown	9	39.440	32963	1523	0.504	0.350	N/A	74355	2.772	N/A	
3	Unknown	9	40.760	6478810	432271	99.023	99.329	N/A	187559	N/A	1.310	

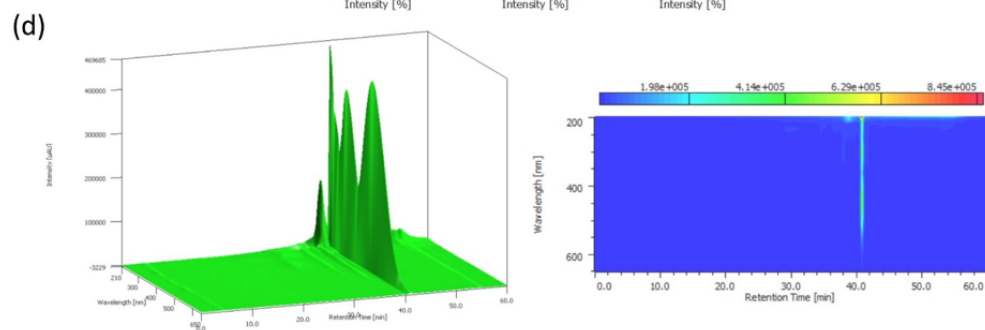
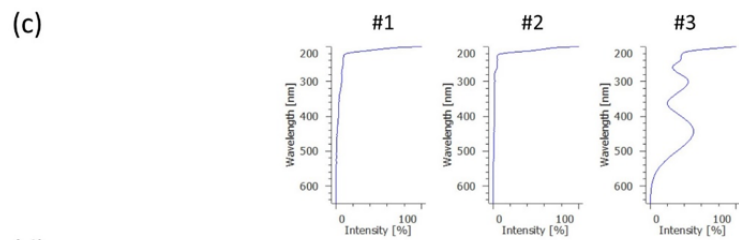
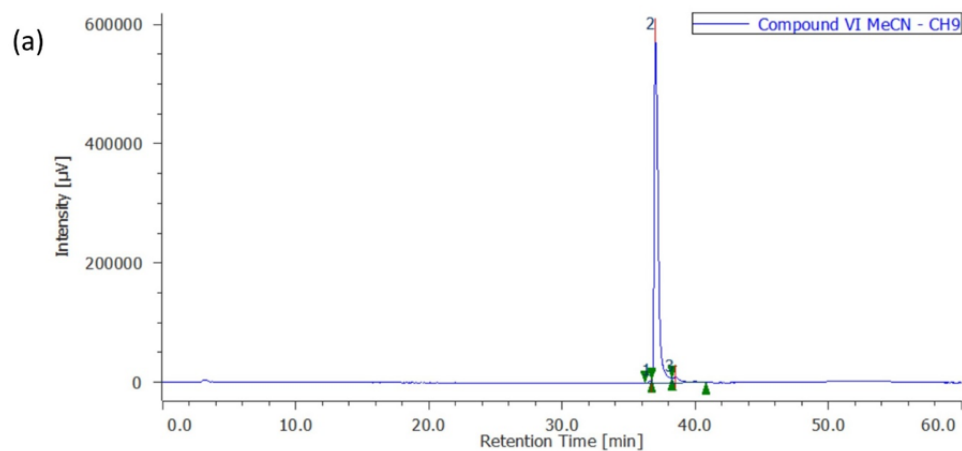


Figure S25: HPLC analysis of molecule (v) utilising method 10-100% MeOH in H₂O. (a) HPLC trace with detection at 450 nm. (b) Analysis of peak area of compounds detected in sample v at 450 nm. (c) Extraction of UV-vis spectra of peaks 1-3 from PDA data. (d) PDA detector data from 200-650 nm shown in 2D and 3D representations.



(b) Analysis of peak area of compounds detected in sample vi at 280 nm.

#	Peak Name	CH	tR [min]	Area [$\mu\text{V}\cdot\text{sec}$]	Height [μV]	Area%	Height%	Quantity	NTP	Resolution	Symmetry Factor	Warning
1	Unknown	9	36.723	52441	4317	0.422	0.713	N/A	N/A	N/A	N/A	
2	Unknown	9	37.007	11945558	590473	96.101	97.547	N/A	84997	N/A	2.049	
3	Unknown	9	38.483	432219	10534	3.477	1.740	N/A	N/A	N/A	N/A	

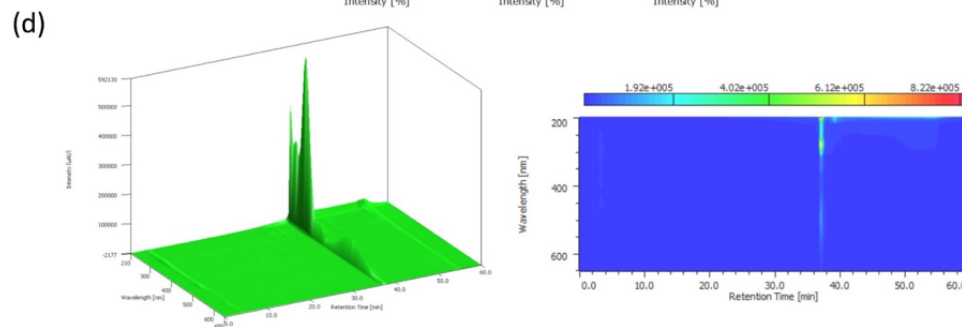
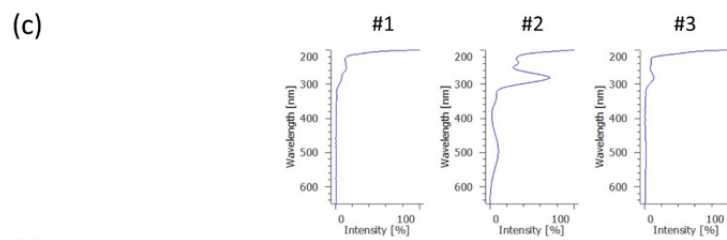


Figure S26: HPLC analysis of molecule (vi) utilising method 10-100% MeOH in H_2O . (a) HPLC trace with detection at 280 nm. (b) Analysis of peak area of compounds detected in sample vi at 280 nm. (c) Extraction of UV-vis spectra of peaks 1-3 from PDA data. (d) PDA detector data from 200-650 nm shown in 2D and 3D representations.

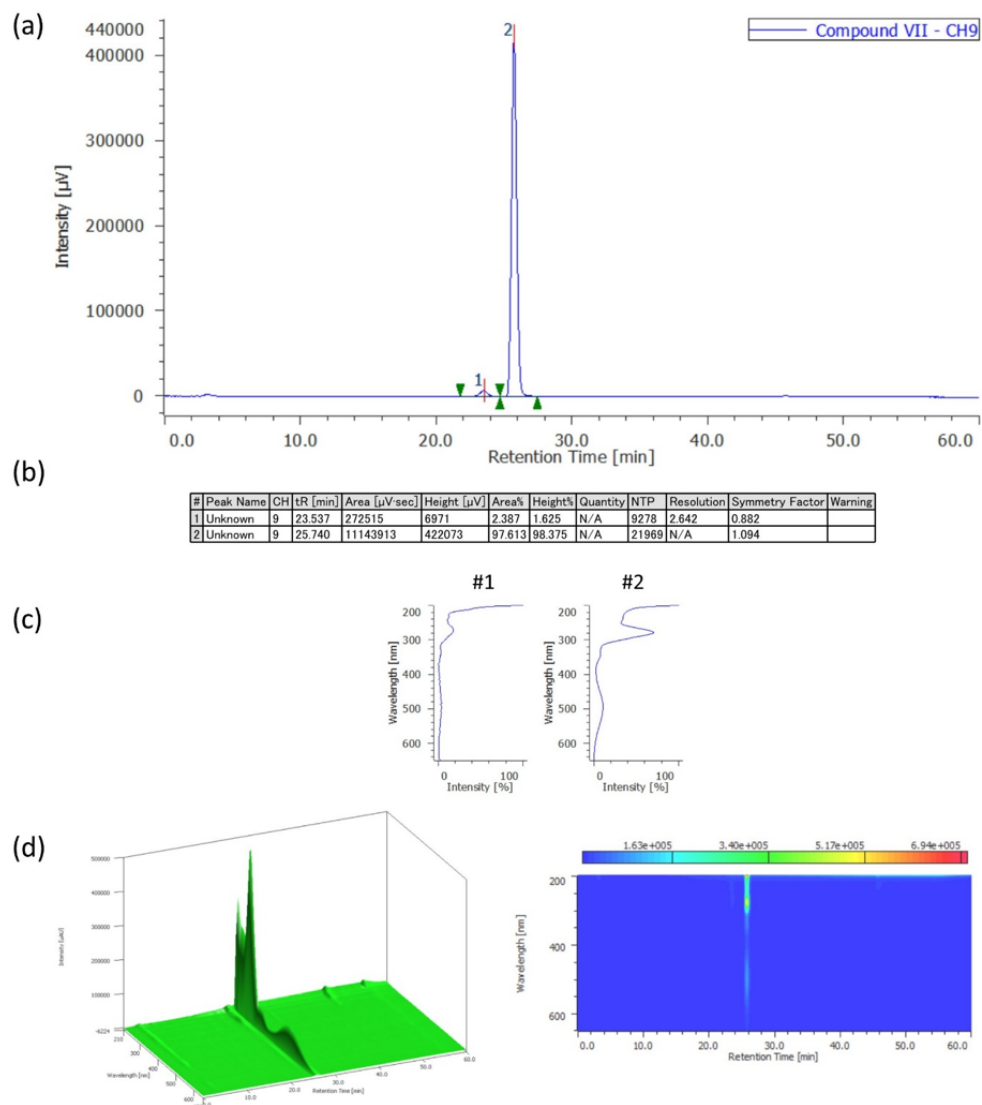


Figure S27: HPLC analysis of molecule (vii) utilising method 50-100% MeOH in H₂O. (a) HPLC trace with detection at 270 nm. (b) Analysis of peak area of compounds detected in sample vii at 270 nm. (c) Extraction of UV-vis spectra of peaks 1-2 from PDA data. (d) PDA detector data from 200-650 nm shown in 2D and 3D representations.

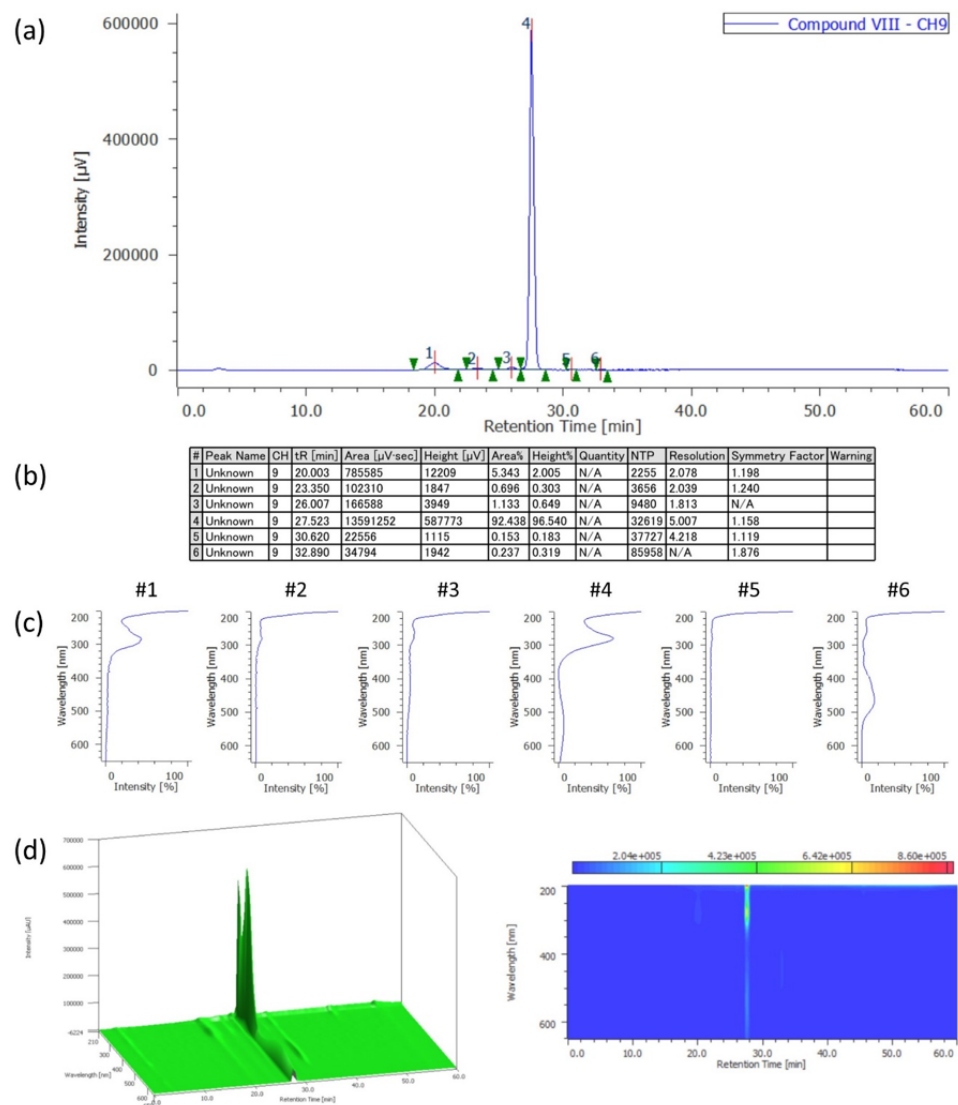


Figure S28: HPLC analysis of molecule (viii) utilising method 50-100% MeOH in H₂O. (a) HPLC trace with detection at 280 nm. (b) Analysis of peak area of compounds detected in sample viii at 280 nm. (c) Extraction of UV-vis spectra of peaks 1-6 from PDA data. (d) PDA detector data from 200-650 nm shown in 2D and 3D representations.